Applied Physics Letters

Structured optical vortices with broadband comb-like optical spectra in Yb:$Y_3Al_5O_{12}$/YVO_4 Raman microchip laser

Cite as: Appl. Phys. Lett. **112**, 161108 (2018); https://doi.org/10.1063/1.5024051
Submitted: 30 January 2018 . Accepted: 08 April 2018 . Published Online: 20 April 2018

Jun Dong, Xiaolei Wang, Mingming Zhang, Xiaojie Wang, and Hongsen He

Structured optical vortices with broadband comb-like optical spectra in Yb:$Y_3Al_5O_{12}$/YVO_4 Raman microchip laser

Jun Dong,[a] Xiaolei Wang, Mingming Zhang, Xiaojie Wang, and Hongsen He
Laboratory of Laser and Applied Photonics (LLAP), Department of Electronic Engineering, Xiamen University, Xiamen 361005, China

(Received 30 January 2018; accepted 8 April 2018; published online 20 April 2018)

Structured optical vortices with 4 phase singularities have been generated in a laser diode pumped continuous-wave Yb:$Y_3Al_5O_{12}$/YVO_4 (Yb:YAG/YVO_4) Raman microchip laser. The broadband comb-like first order Stokes laser emitting spectrum including 30 longitudinal modes covers from 1072.49 nm to 1080.13 nm with a bandwidth of 7.64 nm, which is generated with the Raman shift 259 cm^{-1} of the *c*-cut YVO_4 crystal converted from the fundamental laser around 1.05 μm. Pump power dependent optical vortex beams are attributed to overlap of the Stokes laser field with the fundamental laser field caused by dynamically changing the coupling losses of the fundamental laser field. The maximum output power is 1.16 W, and the optical-to-optical efficiency is 18.4%. This work provides a method for generating structured optical vortices with an optical frequency comb in solid-state Raman microchip lasers, which have potential applications in quantum computations, micro-machining, and information processing. *Published by AIP Publishing.*
https://doi.org/10.1063/1.5024051

Optical vortices carrying optical angular momentum (OAM)[1] have been demonstrated to have potential applications in optical trapping, optical tweezers, quantum telecommunication, and information processing due to their large data-capacity and high security.[2,3] Besides formation of optical vortices with extra-cavity optical elements such as spiral phase plates and computer-generated hologram modulators,[2,3] the optical vortices have been generated in the solid-state lasers by utilizing the thermal lensing effect of the laser gain material,[1,4] doughnut-shaped pump beam, and spot-defect cavity mirror.[5,6] Theoretically predicted optical vortices formed in a frequency-degenerate family of Laguerre-Gauss (LG) modes have been experimentally achieved in an optical pumped Na_2 laser[7,8] and in vertical-cavity surface-emitting semiconductor lasers.[9] Rectangular array beams consisting of a large number of optical vortex pixels have been obtained in a $LiNdP_4O_{12}$ (LNP) laser under asymmetric laser-diode pumping.[10] Optical vortices have been generated in a Nd:$GdCa_4O(BO_3)_3$ self-frequency-doubling microchip laser with high nonlinearity of frequency doubling.[11] Continuous-wave (CW) Raman solid-state lasers have been developed for generating optical vortices[12,13] and expanding the laser wavelength since the first CW Nd:KGW self-Raman laser was demonstrated.[14] The dynamical variation of the output coupling loss for the fundamental field in the intracavity Raman laser has been utilized for generating optical vortices in a CW Nd:$GdVO_4$ self-Raman laser.[15–18] Yb:KGd$(WO_4)_2$,[19] Yb:$KY(WO_4)_2$,[20] and Yb:YVO_4[21] crystals have been used in passively Q-switched lasers to generate a self-Raman laser. However, oscillation of the fundamental and Raman lasers in the same active medium induces severe thermal loading and limits the output power of the self-Raman lasers. With the YVO_4 crystal as a Raman gain medium, Cr^{4+}:YAG passively Q-switched and actively Q-switched Yb:YAG Raman lasers have been demonstrated.[22,23] A multi-wavelength CW Yb:YAG/Nd:YVO_4 Raman microchip laser around 1080 nm has been constructed[24] and proved that the combination of a laser gain medium with a broad emission spectrum and a stimulated Raman scattering (SRS) effect can expand the lasing spectral regime. Raman Microchip lasers (RMLs) with a large Fresnel number and high nonlinearity are ideal arenas for producing stable complex optical vortex fields in a frequency-degenerate family of LG modes because a cooperative frequency-locked multimode Raman laser is easily achieved in a cylindrical symmetry microchip laser cavity pumped with a LG-profile intracavity fundamental laser.

In this letter, watt-level, structured optical vortices in a frequency-degenerated family of LG modes with broadband comb-like optical spectra have been generated in a Yb:YAG/YVO_4 RML by utilizing a heavy-doped Yb:YAG crystal and the SRS effect of the YVO_4 crystal. The bandwidth of the comb-like Raman laser emitting spectrum containing 30 longitudinal modes is more than 7.64 nm. The evolution of the transverse patterns of the Yb:YAG/YVO_4 RML with incident pump power has been studied experimentally and theoretically.

The good mode matching among the pump beam, intracavity fundamental laser beam, and Raman laser is easily achieved in an end-pumped intracavity RML. When a fiber-coupled laser diode with a Gaussian-like beam profile is used as a pump source, the symmetry LG modes are preferably excited in the intracavity RML. In the nonlinearity conversion from a fundamental laser to a Raman laser in the intracavity RML, a common frequency of oscillation is acquired and maintained, and a cooperatively frequency-locked multimode Raman laser is easily obtained for stationary transverse patterns. Therefore, the transverse electrical field in the Yb:YAG/YVO_4 Raman microchip laser can be assumed as a superposition of the $LG_{p,l}$ modes (p and l are

[a]Author to whom correspondence should be addressed: jdong@xmu.edu.cn. Telephone: +86-592-2580004

the radial and angular indexes of the mode) belonging to a specific frequency-degenerate family of LG modes ($2p+|l|=q$ and $q=0,1,2\ldots$). Single TEM_{00} and doughnut $LG_{0,1}$ modes are assumed to oscillate in $2p+|l|=0$ and $2p+|l|=1$ cases, respectively. Besides $LG_{1,0}$, $LG_{0,2}$, and $LG_{0,-2}$ single mode oscillation in the $2p+|l|=2$ case, the stationary multi-mode oscillation can be described as a linearly combination of the three modes[7]

$$F(r,\phi)=E_{1,0}(r,\phi)g_1+E_{0,2}(r,\phi)|g_2|e^{i\theta_2}+E_{0,-2}(r,\phi)|g_3|e^{i\theta_3}, \tag{1}$$

where $E_{1,0}$, $E_{0,2}$, and $E_{0,-2}$ are the electrical fields of $LG_{1,0}$, $LG_{0,2}$, and $LG_{0,-2}$ modes, g_1, g_2, and g_3 are the weights of amplitudes for $LG_{1,0}$, $LG_{0,2}$, and $LG_{0,-2}$ modes, and θ_2 and θ_3 are the rotation angles of the $LG_{0,2}$ and $LG_{0,-2}$ modes, satisfying $\theta_2+\theta_3=\pi$.

The threshold pump power required for Raman laser oscillation with different transverse modes, P_{th}, can be expressed as[15]

$$P_{th}=\frac{(T_S+L_S)L_F}{4l_R}\frac{\lambda_F}{\lambda_P}\frac{A_e}{g_e}\frac{1}{1-e^{-\alpha l}}, \tag{2}$$

where T_S is the mirror transmission for the Stokes field; L_F and L_S are the total round-trip losses for the fundamental and Stokes fields; λ_P and λ_F are the pump and fundamental laser wavelengths; g_e is the effective Raman gain coefficient; α and l are the absorption coefficient and the length of the laser gain medium; l_R is the length of the Raman crystal; and A_e is the effective overlapping area between the fundamental field and the Stokes field, which describes the interaction between the fundamental field and the Stokes field depending on the mode number and can be described as[15]

$$A_e=\frac{1}{\int_{-\infty}^{\infty}\int_{-\infty}^{\infty}I_S(x,y)I_F(x,y)dxdy}, \tag{3}$$

where $I_S(x,y)$ is the normalized Stokes laser intensity distribution and $I_F(x,y)$ is the normalized fundamental laser intensity distribution. Both intensities depend on the order of the LG mode participated and are inversely proportional to the beam waists of the Stokes lasers and fundamental laser, w_S.

Figure 1 depicts the schematics of the experimental setup of a laser diode pumped Yb:YAG/YVO_4 RML and the interference experiment. A fiber-coupled CW 940 nm laser diode with a core diameter of 200 μm and a numerical aperture of 0.22 was served as the pump source. The focused pump spot with a diameter of 100 μm (related to the e^{-2} of the maximum intensity) was located at the rear surface of the Yb:YAG crystal after the collimating and focusing system. A 15 at. % Yb^{3+} ion doped, 1.2-mm-thick Yb:YAG crystal was chosen to enhance laser oscillation at 1050 nm. The rear mirror of the microchip laser was formed with one surface of the Yb:YAG crystal coated with anti-reflection (AR) at 940 nm and high-reflection (HR) at 1030–1100 nm. The Raman gain medium was a 1-mm undoped c-cut YVO_4 crystal. The intracavity surfaces of the Yb:YAG and YVO_4 crystals were coated with AR at 1030–1100 nm. The other surface of the YVO_4 crystal was coated with HR in the fundamental laser radiation region (HR@1030 nm–1060 nm and $R>99.8\%$) and a slight transmission at the first order Stokes laser wavelength ($T\approx0.4\%$ @ 1070–1080 nm) to serve as the output coupling mirror. A pair of copper plates with a 3 mm diameter central aperture was used to hold the tightly attached laser crystal and Raman crystal, which was also served as the heat sink to relieve the thermal accumulation. The experiment was performed at room temperature. The laser beam generated in the Yb:YAG/YVO_4 RML was separated to form a plane wave reference beam with an aperture or a spherical wave reference beam with a lens followed the aperture, as shown in Fig. 1(b). Then, the original laser beam from the RML and the reference beam were interfered on a charge-coupled device (CCD).

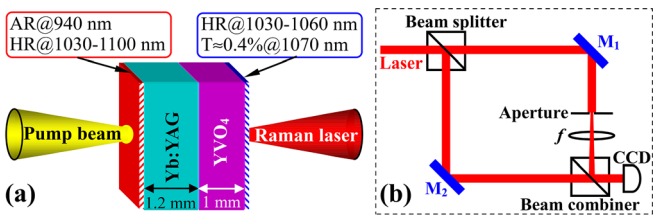

FIG. 1. (a) Schematic diagram for a CW Yb:YAG/YVO_4 RML for generating optical vortices and (b) experimental setup for measuring the interference patterns of the optical vortices.

The laser transverse intensity patterns observed in the Yb:YAG/YVO_4 RML were monitored and recorded with a Thorlabs beam profile analyzer (BC106-VIS). Five different transverse patterns were obtained in the Yb:YAG/YVO_4 RML within the incident pump power (P_{in}) range from 0.9 to 6.28 W. Figure 2(a) shows five typical transverse patterns of the laser at different P_{in} values. A perfect TEM_{00} transverse pattern ($P_{in}=1.25$ W) was obtained when P_{in} was within the range from 0.9 W to 2 W. As P_{in} was increased to over 2 W, the laser transverse pattern switched from the TEM_{00} mode to the doughnut-shaped $LG_{0,1}$ mode ($P_{in}=2.25$ W). The $LG_{1,0}$ mode-like radial symmetric pattern ($P_{in}=4.25$ W) appeared when P_{in} was increased to over 4 W. When P_{in} was further increased higher than 5 W, the complex two-vortex array ($P_{in}=5.94$ W) was obtained and kept for P_{in} from 5 to 6 W. A stable four-vortex array ($P_{in}=6.28$ W) was observed at $P_{in}>6$ W.

The transverse patterns related to the first three LG mode frequency-degenerated families ($q=0$, 1, and 2) in the Yb:YAG/YVO_4 RML oscillating around 1076 nm were theoretically obtained by solving the Raman laser rate equations.[7,9] The theoretically obtained transverse patterns are similar to the experimental observed patterns, as shown in Fig. 2(b). The first family yielded a conventional TEM_{00} mode beam. However, the transverse patterns with optical vortices were formed by numerically calculating the second and third families. The two-vortex array and four-vortex array are the superposition of the $LG_{1,0}$ mode with $LG_{0,2}$ and $LG_{0,-2}$ modes in a LG mode frequency-degenerate family ($2p+|l|=2$).[7] The oscillation of the $LG_{1,0}$ mode Raman laser changes the intracavity fundamental laser field to form a doughnut-shaped distribution, which is favorable for $LG_{0,2}$ and $LG_{0,-2}$ mode Raman laser oscillation. Therefore, the

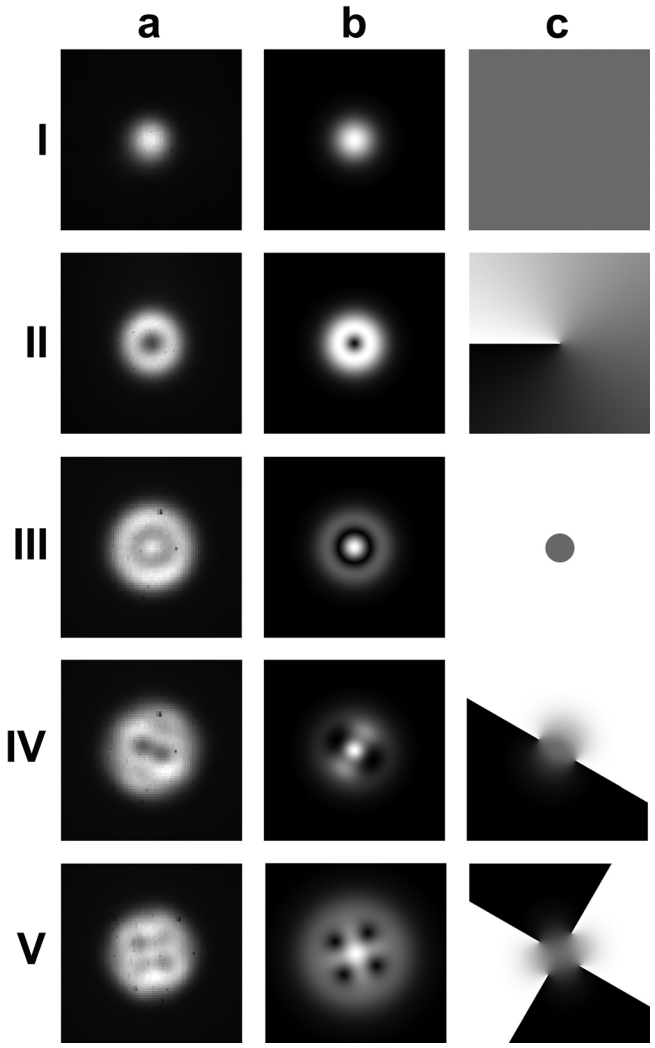

FIG. 2. Transverse patterns observed in the Yb:YAG/YVO_4 RML: experimental (a) (I, 1.25 W; II: 2.25 W; III: 4.25 W; IV: 5.94 W; and V: 6.28 W), theoretical (b) (I: $A_e = 7 \times 10^{-5}$ cm^2 and $P_{th} = 0.63$ W; II: $A_e = 1.3 \times 10^{-4}$ cm^2 and $P_{th} = 1.1$ W; III: $A_e = 1.5 \times 10^{-4}$ cm^2 and $P_{th} = 3.6$ W; IV: $A_e = 3.1 \times 10^{-4}$ cm^2, $P_{th} = 4.8$ W, $g_1 = 0.5$, $g_2 = 1$, and $g_3 = 0.02$; and V: $A_e = 3.2 \times 10^{-4}$ cm^2, $P_{th} = 5.8$ W, $g_1 = 1.7$, $g_2 = 1$, and $g_3 = 1$) and the corresponding phases (c) of the theoretical calculated transverse patterns (b).

weights of the three modes are changed, owing to the mode competition, the g_2 for the $LG_{0,2}$ mode is dominant, while the g_3 for the $LG_{0,-2}$ mode is relatively weak. The g_1 for the $LG_{1,0}$ mode decreases. The weights g_1, g_2, and g_3 for the three modes to form a stable two-vortex array are 0.5, 1, and 0.02. Further increasing the pump power intensity, the increasing output of the three Raman laser modes changes the intracavity fundamental laser fields and makes g_1 increase and g_2 comparable to g_3, and thus, a four-vortex array is formed ($g_1 = 1.7$, $g_2 = 1$, and $g_3 = 1$). Also, the phases of the calculated patterns are plotted in Fig. 2(c). From Fig. 2(c), we can see that the obtained different optical vortices have the phase singularities, which satisfy the phase gradient about the singularity $\oint \nabla\Phi \cdot dl = \pm 2m\pi$, where m is the topological charge of the vortex. The vortices appeared in the doughnut-shaped $LG_{0,1}$ mode, two-vortex array, and four-vortex array are generally considered to possess 1, 2, and 4 phase singularities, respectively.

Interference experiments were conducted to verify the phase helicity of the observed optical vortices. Figure 3 shows the measured interference fringes and spiral patterns of the $LG_{0,1}$ mode and two-vortex array emitted by the RML. A single fringe splits into two fringes, as shown in Fig. 3(a), which verifies that the output $LG_{0,1}$ mode laser beam possesses a phase singularity at the fork dislocation and the emitting laser is an optical vortex beam with topological charge $m = 1$. As shown in Fig. 3(b), a clear spiral fringe with right-handedness further confirms the helical phase distribution of the doughnut-shaped transverse pattern. Two forklike fringes with opposite directions were observed when the two-vortex array beam was interfered with a plane wave reference beam, as shown in Fig. 3(c), which gives a clear evidence for the two-vortex array possessing two phase singularities with topological charge $m = \pm 1$. The measured interference patterns of two dark holes with the spherical wave reference beam clearly show spiral structures with two opposite handedness, as shown in Figs. 3(d) and 3(e), respectively, which confirms the helical phase nature of the two-vortex array laser beam.

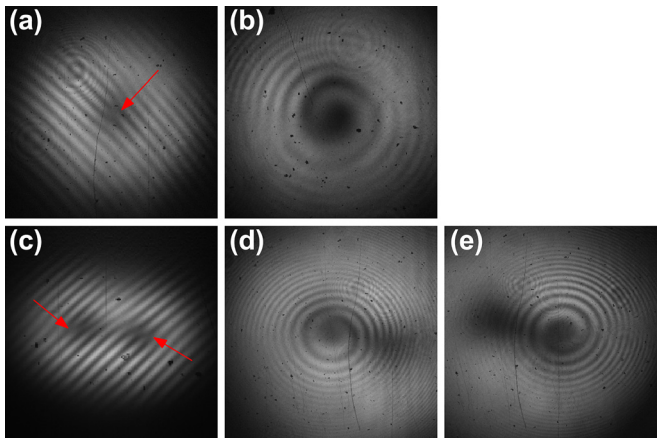

FIG. 3. Interference patterns: (a) fork interference pattern and (b) spiral interference pattern of the doughnut mode and (c) fork interference pattern and spiral interference patterns for the left dark hole (d) and the right dark hole (e) of the two-vortex array.

The pump power dependence of the output power and optical efficiency in the CW Yb:YAG/YVO_4 RML is given in Fig. 4. The SRS threshold pump powers for TEM_{00}, $LG_{0,1}$, $LG_{1,0}$, the two-vortex array, and the four-vortex array

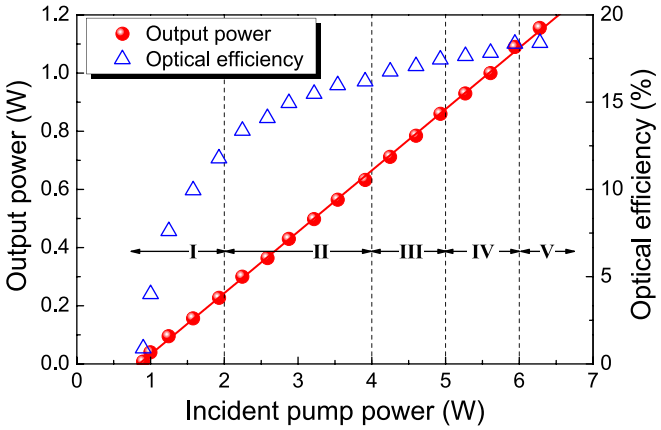

FIG. 4. Output power and optical efficiency of the CW Yb:YAG/YVO_4 RML versus the incident pump power. I: TEM_{00}, II: doughnut-shaped vortex, III: $LG_{1,0}$, IV: two-vortex array, and V: four-vortex array.

in the Yb:YAG/YVO_4 RML were measured to be 0.9, 2, 4, 5, and 6 W, respectively. Although the transverse pattern was changed with an increase in P_{in}, the linear increase in the Raman laser output power with P_{in} was observed. The slope efficiency was approximately 21%. The output power and the corresponding incident pump power range for three different vortices are summarized in Table I. The maximum Raman laser output power was 1.16 W at $P_{in} = 6.28$ W. The optical efficiency was as high as 18.4%, which was 4.4 times of that obtained in the Yb:YAG/Nd:YVO_4 RML.[24] The dramatic improvement of Raman laser optical efficiency in the Yb:YAG/YVO_4 RML was mainly attributed to the heavy-doped Yb:YAG crystal and YVO_4 Raman gain crystal utilized in the experiment. The heavy-doped Yb:YAG crystal is preferable for generating the fundamental laser at 1050 nm owing to the enhanced gain at 1050 nm and strong reabsorption at 1030 nm. The perfect lattice structure of undoped YVO_4 crystals is more favorable for SRS generation than that of Nd^{3+}-ion doped YVO_4 crystals. There was no output power rollover for the Yb:YAG/YVO_4 RML, suggesting that the output power of the Yb:YAG/YVO_4 RML should be scaled by further increasing pump power.

The theoretical calculated SRS threshold pump powers of different transverse patterns as a function of the intracavity Raman laser beam waist are shown in Fig. 5. The parameters for the theoretical calculation are used as follows: $g_e = 4.5$ cm/GW, $l_R = 1$ mm, $l = 1.2$ mm, $\alpha = 15\ \mathrm{cm}^{-1}$, $\lambda_P = 940$ nm, $\lambda_F = 1050$ nm, $w_F = 50\ \mu$m, $T_S = 0.4\%$, $L_S = 0.2\%$, and $L_F = 0.2\%$. The calculated results indicate that the SRS threshold pump powers for different transverse patterns strongly depend on the intracavity Raman laser beam waist when the fundamental laser beam waist and profile are set. The calculated SRS threshold pump powers for different transverse patterns are $P_{th\_TEM00} < P_{th\_LG0,1} < P_{th\_LG1,0} < P_{th\_2\text{-vortex}} < P_{th\_4\text{-vortex}}$ when the intracavity Raman laser beam waist is set. The same tendency was observed for the SRS threshold pump powers of different transverse patterns in the experiment (solid symbols in Fig. 5). The discrepancies between calculated threshold pump power and experimental results are caused by rough estimation of the losses for different participating modes and neglection of the gain decrease induced by the thermal effect in the theoretical calculations.

The laser emitting spectra of the vortex beams generated in the RML were measured with an Anritsu optical spectral analyzer (MS9740A). The broadband laser emitting spectra around 1076 nm have been observed when P_{in} exceeds the threshold pump power for Raman laser oscillation. The 259 cm^{-1} Raman shift line of the *c*-cut YVO_4 crystal is employed to convert the fundamental laser at 1.05 μm to the Raman laser at 1076 nm. Figure 6 depicts some typical laser emitting spectra of the Yb:YAG/YVO_4 RML at different pump power levels. No fundamental laser observed in the Yb:YAG/YVO_4 RML indicated that the intracavity fundamental laser was clamped and fully converted to the Raman laser. When P_{in} was further increased to 4.9 W, extra longitudinal modes emerged around 1073 nm, as shown in Fig. 6(b), which was induced by the asymmetric emission spectrum of the Yb:YAG crystal around 1.05 μm.[25] The longitudinal mode number and the spectral bandwidth increase with P_{in}. When P_{in} was further increased to over 6 W, the laser emitting spectra of the RML at 1073 nm and 1076 nm were connected together and covered from 1072.49 nm to 1080.13 nm with a bandwidth of 7.64 nm and 30 longitudinal modes, as shown in Fig. 6(d). The corresponding Fourier transform limited pulse duration is approximately 159 fs. The structured four-vortex array with a broadband comb-like spectrum has potential applications on increasing data storage capacity and generating femtosecond laser pulses with self-mode locking.

In conclusion, the structured optical vortices with broadband comb-like laser spectra have been generated in the

TABLE I. Incident pump power (P_{in}) and output power (P_{out}) of different optical vortices.

Vortex	P_{in} (W)	P_{out} (W)
Doughnut vortex	2–4	0.3–0.63
Two-vortex array	5–6	0.9–1.1
Four-vortex array	>6	1.16

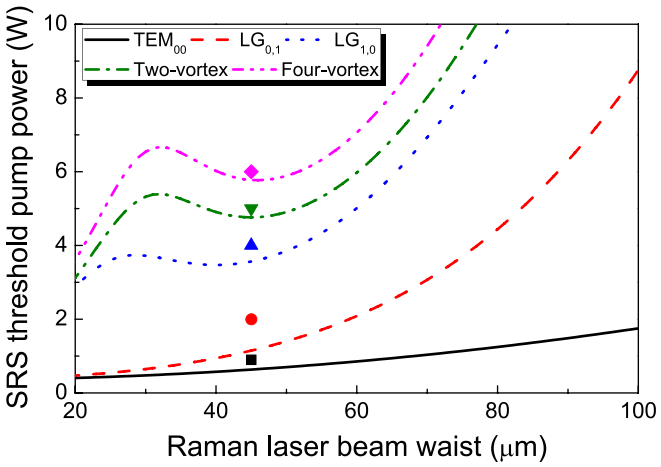

FIG. 5. Theoretical calculated SRS threshold pump power of different patterns formed in the Yb:YAG/YVO_4 RML as a function of the Raman laser beam waist. The experimentally obtained SRS threshold pump powers for different transverse patterns are plotted in the solid dots.

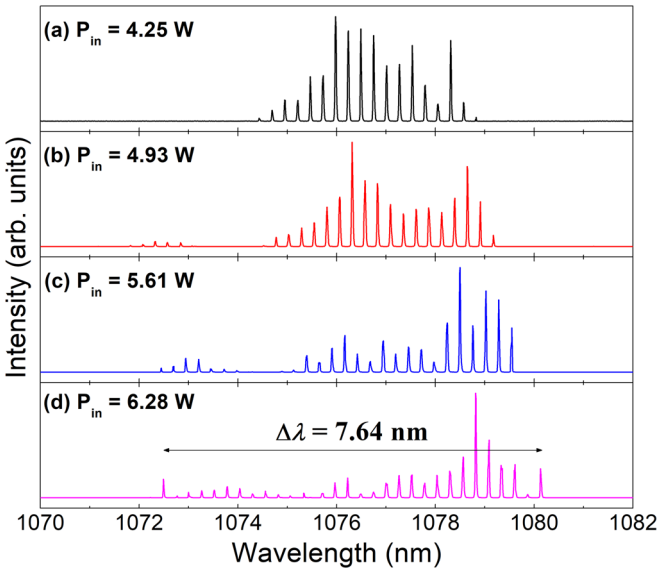

FIG. 6. Laser emitting spectra of the Yb:YAG/YVO_4 RML at different incident pump powers.

Yb:YAG/YVO_4 RML by utilizing the SRS nonlinear optical process of the YVO_4 crystal and heavy-doped Yb:YAG crystal. The doughnut-shaped $LG_{0,1}$ mode, two-vortex array, and four-vortex array have been obtained depending on the applied pump power. The comb-like Raman laser emitting spectrum covers from 1072.49 nm to 1080.13 nm with a spectral bandwidth of 7.64 nm and 30 equidistant longitudinal modes. The Raman laser output power of 1.16 W with the optical-to-optical efficiency of 18.4% was obtained. Formation of optical vortices in the Yb:YAG/YVO_4 RML is determined by the dynamic change in the output coupling loss for the fundamental laser with conversion to the Raman laser. This work paves a road to generate optical vortices with an optical frequency comb in miniature solid-state lasers.

This work was supported by the National Natural Science Foundation of China (61275143 and 61475130) and the Program for New Century Excellent Talents in University (NCET-09-0669).

[1]M. Okida, T. Omatsu, M. Itoh, and T. Yatagai, Opt. Express **15**, 7616 (2007).
[2]M. W. Beijersbergen, R. P. C. Coerwinkel, M. Kristensen, and J. P. Woerdman, Opt. Commun. **112**, 321 (1994).
[3]C. Paterson and R. Smith, Opt. Commun. **124**, 121 (1996).
[4]M. Okida, Y. Hayashi, T. Omatsu, J. Hamazaki, and R. Morita, Appl. Phys. B-Lasers Opt. **95**, 69 (2009).
[5]J. W. Kim and W. A. Clarkson, Opt. Commun. **296**, 109 (2013).
[6]A. Ito, Y. Kozawa, and S. Sato, J. Opt. Soc. Am. A **27**, 2072 (2010).
[7]M. Brambilla, F. Battipede, L. A. Lugiato, V. Penna, F. Prati, C. Tamm, and C. O. Weiss, Phys. Rev. A **43**, 5090 (1991).
[8]C. Tamm and C. O. Weiss, Opt. Commun. **78**, 253 (1990).
[9]J. Scheuer and M. Orenstein, Science **285**, 230 (1999).
[10]K. Otsuka and S. C. Chu, Opt. Lett. **34**, 10 (2009).
[11]H. H. Yu, H. J. Zhang, Z. P. Wang, J. Y. Wang, Z. B. Pan, S. D. Zhuang, and D. Y. Tang, Appl. Phys. Lett. **99**, 241102 (2011).
[12]J. T. Murray, W. L. Austin, and R. C. Powell, Opt. Mater. **11**, 353 (1999).
[13]P. Dekker, H. M. Pask, D. J. Spence, and J. A. Piper, Opt. Express **15**, 7038 (2007).
[14]A. A. Demidovich, A. S. Grabtchikov, V. A. Lisinetskii, V. N. Burakevich, V. A. Orlovich, and W. Kiefer, Opt. Lett. **30**, 1701 (2005).
[15]D. J. Spence, IEEE J. Sel. Top. Quantum Electron. **21**, 1400108 (2015).
[16]A. J. Lee, T. Omatsu, and H. M. Pask, Opt. Express **21**, 12401 (2013).
[17]A. J. Lee, C. Zhang, T. Omatsu, and H. M. Pask, Opt. Express **22**, 5400 (2014).
[18]A. J. Lee, H. M. Pask, and T. Omatsu, Appl. Phys. B-Lasers Opt. **122**, 64 (2016).
[19]A. A. Lagatsky, A. Abdolvand, and N. V. Kuleshov, Opt. Lett. **25**, 616 (2000).
[20]A. S. Grabtchikov, A. N. Kuzmin, V. A. Lisinetskii, V. A. Orlovich, A. P. Voitovich, A. A. Demidovich, H. J. Eichler, and A. N. Titov, Quantum Electron. **33**, 165 (2003).
[21]V. E. Kisel, A. E. Troshin, N. A. Tolstik, V. G. Shcherbitsky, N. V. Kuleshov, V. N. Matrosov, T. A. Matrosova, and M. I. Kupchenko, Appl. Phys. B-Lasers Opt. **80**, 471 (2005).
[22]W. Jiang, S. Zhu, W. Chen, H. Lin, Y. Liu, Z. Chen, G. Zhang, Y. Chen, Y. Duan, and Z. Chen, IEEE Photonics Technol. Lett. **27**, 1080 (2015).
[23]W. Jiang, Z. Li, S. Zhu, H. Yin, Z. Chen, G. Zhang, and W. Chen, Opt. Express **25**, 14033 (2017).
[24]X.-L. Wang, J. Dong, X.-J. Wang, J. Xu, K.-I. Ueda, and A. A. Kaminskii, Opt. Lett. **41**, 3559 (2016).
[25]J. Dong, A. Shirakawa, K. Ueda, H. Yagi, T. Yanagitani, and A. A. Kaminskii, Appl. Phys. Lett. **89**, 091114 (2006).